Originally published as:

Persistent Octahedral Coordination in Amorphous GeO₂ Up to 100 GPa by Kβ'' X-Ray Emission Spectroscopy

G. Spiekermann,[1,2,3,*] M. Harder,[2] K. Gilmore,[4] P. Zalden,[5] Ch. J. Sahle,[4] S. Petitgirard,[6] M. Wilke,[1] N. Biedermann,[1,5]
C. Weis,[7] W. Morgenroth,[8] J. S. Tse,[9] E. Kulik,[2] N. Nishiyama,[2,10] H. Yavaş,[2,11] and C. Sternemann[7]

[1]*Institut für Geowissenschaften, Universität Potsdam, 14476 Potsdam, Germany*
[2]*Deutsches Elektronen-Synchrotron DESY, 22607 Hamburg, Germany*
[3]*Deutsches GeoForschungsZentrum GFZ, 14473 Potsdam, Germany*
[4]*European Synchrotron Radiation Facility, 71 Avenue des Martyrs, 38043 Grenoble, France*
[5]*European XFEL, 22869 Schenefeld, Germany*
[6]*Universität Bayreuth, Bayerisches Geoinstitut BGI, 95447 Bayreuth, Germany*
[7]*Fakultät Physik/DELTA, Technische Universität Dortmund, 44221 Dortmund, Germany*
[8]*Institut für Geowissenschaften, Universität Frankfurt, 60438 Frankfurt am Main, Germany*
[9]*Department of Physics, University of Saskatchewan, Saskatoon, Saskatchewan S7N 5E2, Canada*
[10]*Tokyo Institute of Technology, 2-12-1 Ookayama, Meguro-ku, Tokyo 152-8550, Japan*
[11]*Linac Coherent Light Source, SLAC National Accelerator Laboratory,
2575 Sand Hill Road, Menlo Park, California 94025, USA*

We measure valence-to-core x-ray emission spectra of compressed crystalline GeO₂ up to 56 GPa and of amorphous GeO₂ up to 100 GPa. In a novel approach, we extract the Ge coordination number and mean Ge-O distances from the emission energy and the intensity of the Kβ'' emission line. The spectra of high-pressure polymorphs are calculated using the Bethe-Salpeter equation. Trends observed in the experimental and calculated spectra are found to match only when utilizing an octahedral model. The results reveal persistent octahedral Ge coordination with increasing distortion, similar to the compaction mechanism in the sequence of octahedrally coordinated crystalline GeO₂ high-pressure polymorphs.

Subject Areas: Condensed Matter Physics, Geophysics,
Materials Science

I. INTRODUCTION

The structure of amorphous and crystalline GeO₂ at high pressure is of interest due to its use in technical glasses and due to fundamental questions related to the compaction mechanism on the atomic scale in this archetypal network forming system [1–13]. The compaction mechanism in the amorphous phase has important geophysical and geochemical implications, as GeO₂ is a structural analog of SiO₂, the main component in silicate melts present in Earth's mantle. If amorphous GeO₂ and SiO₂ would reach or even exceed the density of crystalline polymorphs by atomic scale compaction, this could help to explain geophysical observations that point towards buoyantly stable silicate melts at various depths in Earth's mantle [14,15]. It is therefore important to understand the compaction

mechanism in an experimentally accessible analog material like amorphous GeO₂ in order to assess the differences from and similarities to the mechanisms in crystalline polymorphs.

The most important parameter to describe the structure of compressed amorphous GeO₂ and its crystalline polymorphs is the average number of nearest oxygen neighbors to germanium, i.e., its average coordination number (CN). There is a well-known pressure lag in the average CN between compressed amorphous GeO₂ and stable crystalline GeO₂ polymorphs: The CN in GeO₂ polymorphs stable at pressures above 5 GPa is six, while the CN of the amorphous state gradually increases from four to six in an extended pressure range up to 20 GPa [1,3–5,8,10–12,16]. In the similar case of SiO₂, the first stable polymorph with CN of six appears at 7 GPa, whereas compressed amorphous SiO₂ reaches an average CN of six only between 40 and 60 GPa [15,17]. Can the lag in CN between the amorphous and the crystalline state be reversed at higher pressures, as two groups showed in their recent x-ray diffraction studies on GeO₂ [1] and SiO₂ [18]? In amorphous GeO₂, an increase of the CN from six to seven has been reported between 40 and 60 GPa by XRD [1].

This CN evolution beyond 6-fold does not match the one observed for crystalline GeO_2 polymorphs, which have a CN of six up to at least 110 GPa [19,20]. Moreover, the recent *ab initio* molecular dynamics (AIMD) study of Du and Tse on amorphous GeO_2 has found that the average germanium CN has a dominant fraction above six only for pressures larger than 80 GPa [21]. In the case of amorphous SiO_2, the conclusions of different studies concerning the CN at high pressure diverge in a similar fashion, with recent XRD data showing a CN beyond six [18], contradicting previous XRD data [22], *ab initio* molecular dynamics calculations [23], spectroscopic measurements at the Si L-edge [15], and density measurement [24]. Thus, there is fundamental ambiguity in the compressional behavior of these network-forming systems at extreme pressure in general.

In this study, we address the ambiguity in the average germanium CN in compressed amorphous GeO_2 by a new approach on the basis of measured and computed valence-to-core x-ray emission spectroscopy (VTC XES) spectra of compressed GeO_2. VTC XES has been mostly applied to $3d$ transition metal molecular complexes, where it is known to provide insight into the spin state and the type of the bonding ligand [25–34]. There have been only a few studies on nonmolecular crystalline compounds [35–39]. Here, we demonstrate the potential of this technique for structural characterization of the amorphous state. We find that compressed amorphous GeO_2 remains in persistent sixfold coordination up to 100 GPa, with the GeO_6 octahedra being increasingly distorted with pressure.

II. OCTAHEDRAL DISTORTION

The average Ge-O distance is a second important parameter to describe amorphous GeO_2, linked to the CN by the principles of bond valence theory and increases with increasing CN [40,41]. At constant CN, increasing pressure causes shortening of the average Ge-O bond, determined by the bulk modulus of the coordinating polyhedron [42]. We consider *mean* Ge-O distance unless indicated otherwise, defined as the arithmetic mean of all Ge-O distances in the first coordination shell.

The distortion of the GeO_6 octahedron of six oxygen neighbors surrounding the germanium is a third parameter important to evaluate in both amorphous GeO_2 and the crystalline polymorphs sequence of rutilelike GeO_2 (r-GeO_2), $CaCl_2$-like, α-PbO_2-like and FeS_2-like GeO_2 [19,43]. Octahedral distortion is described by the variance of both Ge-O distance and bond angles in the GeO_6 octahedra (see Ref. [44], and references therein). The variance in bond length increases from 1% in rutilelike GeO_2 to 5% in α-PbO_2-like GeO_2, but drops to zero in cubic FeS_2-like GeO_2. The bond angle variance increases from $25°$ in high-pressure rutilelike to $80°$ in FeS_2-like GeO_2, passing through a minimum in $CaCl_2$-like GeO_2 at 28 GPa. Overall,
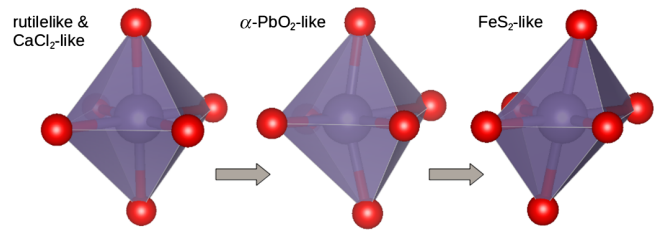

FIG. 1.   The distortion of the GeO_6 octahedron in the sequence of crystalline high-pressure GeO_2 polymorphs rutilelike GeO_2, $CaCl_2$-like, α-PbO_2-like, and FeS_2-like GeO_2.

there is a trend of increasing octahedral distortion in the high-pressure polymorphs of GeO_2 (Fig. 1) [44].

The increasing octahedral distortion from one polymorph to the next allows the GeO_6 octahedra to maintain a mean Ge-O distance larger than those that would be reached by isostructural compression. For instance, while the bulk modulus of the GeO_6 octahedron in rutilelike GeO_2 is about 300 GPa [42], the increasing GeO_6 distortion in the sequence of crystalline high-pressure GeO_2 polymorphs allows the average Ge-O distance to decrease less, resulting in a much higher effective octahedral bulk modulus. While the octahedral distortion in compressed amorphous GeO_2 is not directly accessible to measurement, it can be inferred from the comparison of the mean Ge-O distance to the one of crystalline high-pressure GeO_2 polymorphs, as we show below. While no crystalline GeO_2 or SiO_2 polymorph with a CN above six has been found experimentally [19,20], GeO_2 in the $PbCl_2$-like, cotunnite structure with a CN of nine has been proposed and investigated in an *ab initio* study as a candidate polymorph beyond FeS_2-like GeO_2 [13].

III. $K\beta''$ EMISSION LINE

The $K\beta''$ emission line (EL) is part of the VTC XES spectra of GeO_2 and many other chemical systems that combine $3d$ transition metals or adjacent elements with ligands from the second or third row of the periodic table. Figure 2 shows measured (top) and calculated (bottom) VTC XES spectra of q-GeO_2 and r-GeO_2 with the $K\beta_5$, $K\beta''$, and $K\beta_2$ emission lines. The $K\beta_5$ EL originates from the $3d$ orbitals and the $K\beta_2$ EL originates from overlapping $4p$ and $4s$ to $1s$ transitions. The $K\beta''$ EL reflects the binding energy of the oxygen $2s$ electrons, which are essentially nonbonding in many systems [25,26,45]. However, a few percent mixing of Ge $4p$ orbitals with oxygen $2s$, as evident from the projected density of states, gives rise to the $K\beta''$ EL in germanium K-shell spectra. Because of the predominant oxygen $2s$ character, the $K\beta''$ EL is also commonly referred to as a "crossover transition." It is therefore absent in the VTC XES spectrum of elemental Ge (Fig. 2, top).

The intensity of the $K\beta''$ EL is a measure of the cation-ligand distance due to the increasing extent of hybridization
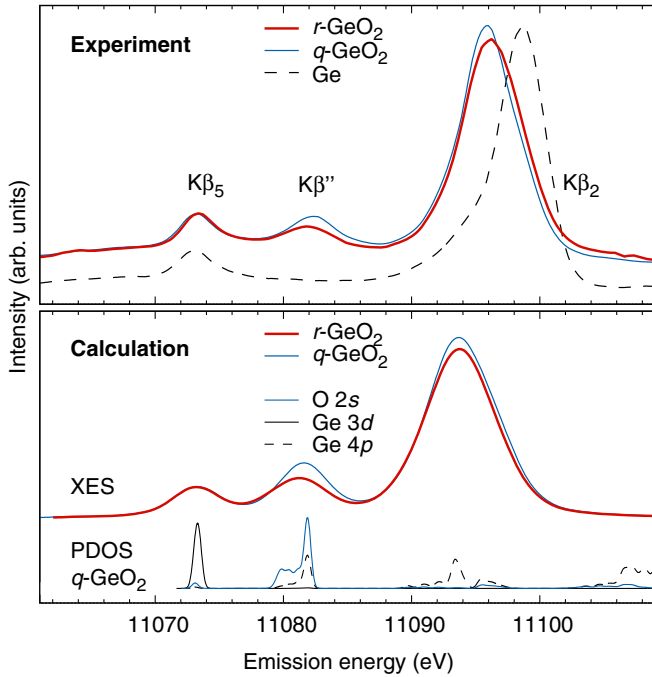
FIG. 2. Top: Measured germanium VTC XES spectra of quartzlike and rutilelike GeO_2. The spectrum of elemental Ge is shown for comparison. Bottom: Bethe-Salpeter spectral calculations, aligned to the $K\beta_5$ emission line. The projected density of states of q-GeO_2 demonstrates the oxygen $2s$ character of the $K\beta''$ emission line.

of oxygen $2s$ electrons with cation p valence electrons, here Ge $4p$, with decreasing cation-ligand distance [25–27,46]. Accordingly, the $K\beta''$ of q-GeO_2 with an average Ge-O distance of 1.74 Å at ambient pressure is more intense than the one of r-GeO_2 with an average bond length of 1.88 Å. The emission energy of the $K\beta''$ EL differs by about 0.7 eV at ambient pressure between CN = 4 in q-GeO_2 and CN = 6 in r-GeO_2 (Fig. 2). Measurement of the shift of the $K\beta''$ in compressed amorphous GeO_2 allows for tracking the germanium CN by comparison to the shift of crystalline GeO_2 references of different CN at high pressure. The average Ge-O distance is extracted from the intensity change of the $K\beta''$ EL, by comparison to measured and computed spectra of crystalline references.

IV. MATERIALS AND EXPERIMENTAL METHODS

We loaded amorphous GeO_2 (a-GeO_2 [47]) (three independent loadings), polycrystalline quartzlike GeO_2 (q-GeO_2) (two independent loadings), and rutilelike GeO_2 (r-GeO_2, [48]) into diamond anvil cells (DACs). r-GeO_2 was measured at high pressure as a reference material of CN = 6. Panoramic DACs with a pair of anvils of different culet sizes, namely 400 and 300 μm for pressures below 30 GPa and 300 and 200 μm above, were used. The use of different culets is important for the

acquisition of the emission signal, as the penetration depths of the different culets into the 200-μm-thick rhenium gasket leads to a lower gasket indentation wall on the side of the larger culet. The sample chambers of 100 and 80 μm diameter, respectively, were completely filled with sample powder. The pressure was determined from the shift of the fluorescence line of ruby chips inside the sample chamber [49]. We estimate the measurement error in pressure to be about ± 1 GPa below 20 GPa and about ± 2 GPa for pressures above 20 GPa. Elemental germanium was measured at ambient pressure for reference.

Measurements of the XES were performed at beam line P01 at DESY, Germany. The incident beam of 12.5 keV was monochromatized with a Si(111) monochromator and focused by a Kirkpatrick-Baez mirror to $7 \times 15\ \mu$m^2 FWHM (V $\times$ H). It entered the DAC through the diamond with the smaller culet size. We collected the emission signal at near-90° scattering angle with an energy-dispersive von Hamos-type spectrometer [37,50] in such a way that the emitted radiation passed through the side of the larger diamond, a few degrees past the gasket indentation wall. Eight cylindrically bent Si(nn0) crystals with 0.5 m bending radius dispersed the signal onto a Pilatus 100k detector with a pixel size of 172 μm. The detection with Si(660) planes and a mean Bragg angle of 61° resulted in a spectral bandwidth of about 180 eV with an energy resolution of about 1 eV. We used the Si(880) Bragg reflection to determine the dispersion of each analyzer crystal via detecting the elastic scattering at various settings of the monochromator energy. The acquisition time of the VTC XES spectra was 20 min for each pressure step. After summing the signal of the analyzers, we subtracted a second-order polynomial background.

V. COMPUTATION OF SPECTRA

We computed the VTC XES spectra of crystalline GeO_2 polymorphs by numerical solution of the Bethe-Salpeter equation, as implemented in the OCEAN code [51]. The ground state electronic structure was computed within the theoretical framework of density functional theory as implemented in the QUANTUM ESPRESSO package [52], using the local density approximation for the exchange-correlation functional.

For the crystalline structures of GeO_2 at ambient and high pressure, we used experimentally determined structures of q-GeO_2 (CN = 4) and r-GeO_2, $CaCl_2$-like, α-PbO_2-like, and FeS_2-like GeO_2 (all CN = 6) [19,43,53]. q-GeO_2 with CN of four amorphizes above 5 GPa [53]. In order to obtain spectra of CN = 4 above 5 GPa, we stepwise downscaled the volume of the unit cell of highest pressure of 4.6 GPa [53]. The unit cell of cotunnite-structured $PbCl_2$-like GeO_2 with CN = 9 [13] was also scaled in volume. In the scaling of the volume of the unit cell all proportions were maintained. At each scaling step, we computed the spectrum and the pressure from the stress
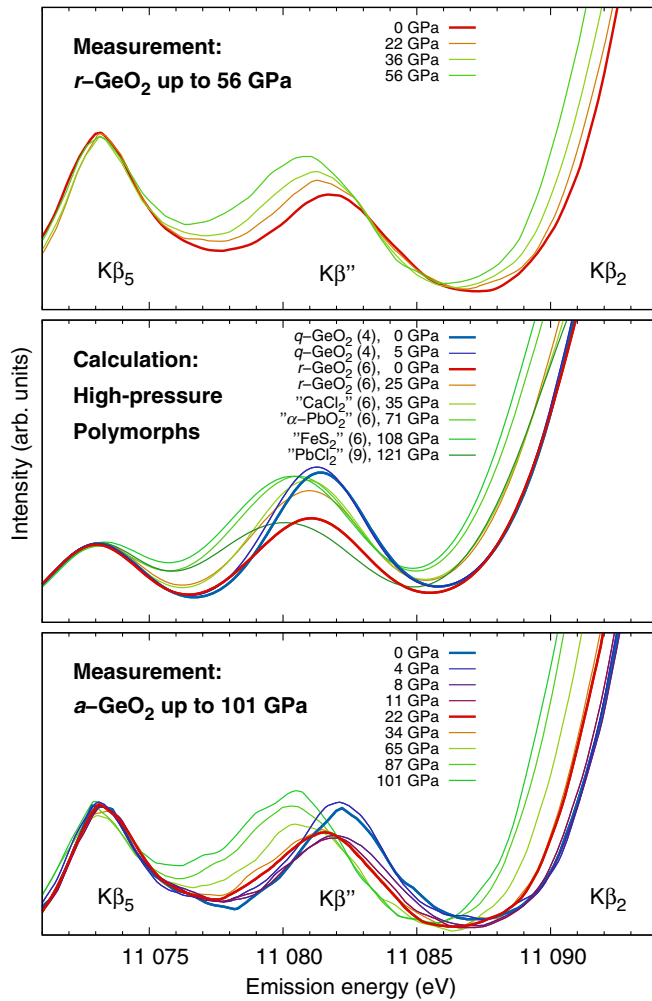
FIG. 3.   Top: Measured spectra of rutilelike GeO_2, compressed to 56 GPa. Middle: Calculated VTC XES spectra of the sequence of crystalline high-pressure GeO_2 polymorphs. Bottom: Measured spectra of amorphous GeO_2, compressed up to 101 GPa. The spectra are normalized to the area of the $K\beta_5$ EL.

tensor. All computed pressures were corrected by subtraction of the linear, pressure-dependent mismatch found for the known crystalline high-pressure GeO_2 polymorphs used in this study. In this way, we achieved agreement between experimental and computed pressure with a deviation below 5 GPa, or in a few cases 8 GPa. The calculated spectra were convoluted and shifted for visualization to match the experimental emission energy of the $K\beta_5$ EL (Fig. 3, middle).

Both emission energy and intensity of the $K\beta''$ EL in germanium oxides can be conveniently expressed relative to the $K\beta_5$ EL, which serves as an internal energy and intensity calibrant. The $K\beta_5$ EL is almost constant in both emission energy and intensity for germanium oxides, due to the localization and semicore character of the filled $3d$ shell. The energy of the $K\beta_5$ EL is equal for the two polymorphs of GeO_2, and shifted by less than 0.1 eV in

elemental germanium (Fig. 2). Energy shifts of the $K\beta''$ EL in the VTC XES spectra of GeO_2 are thus described as energy difference ΔE between the $K\beta''$ and $K\beta_5$ ELs, $\Delta E = E(K\beta'') - E(K\beta_5)$. Changes in the intensity of $K\beta''$ are expressed as the ratio of the intensities $RI = I(K\beta'')/I(K\beta_5)$.

VI. RESULTS AND DISCUSSION

The evolution of the $K\beta''$ EL of compressed r-GeO_2 up to 56 GPa is shown in Fig. 3 (top). The $K\beta''$ EL intensity increases and shifts continuously, reflecting the decreasing mean Ge-O distance and the increasing binding energy of oxygen $2s$ electrons with pressure. Selected computed spectra of crystalline ambient and high-pressure GeO_2 polymorphs are shown in Fig. 3 (middle). With increasing pressure, both within a given structure *and* across structural transitions, the $K\beta''$ EL shifts to higher binding energies. Its intensity is highest for q-GeO_2 (CN = 4) and lowest for $PbCl_2$-like GeO_2 (CN = 9) at 121 GPa, thereby reflecting the increasing mean Ge-O distance with increasing CN. Selected VTC XES spectra of compressed a-GeO_2 are shown in Fig. 3 (bottom). While the $K\beta_5$ EL is constant in position within the measurement uncertainty, the $K\beta''$ EL shifts with pressure by more than 2 eV between 0 and 100 GPa. Its intensity initially decreases to a minimum at 15 GPa and then continuously increases up to 100 GPa. Compression of q-GeO_2 shows a similar behavior (not shown). In the following, we evaluate the measured spectra in terms of ΔE and RI, as defined above, which allows us to determine the average germanium CN and average Ge-O distance.

A. Germanium coordination number

Figure 4 (top) shows the ΔE, i.e., the position of the $K\beta''$ EL with respect to $K\beta_5$, from calculated spectra of crystalline polymorphs of CN = 4, 6, and 9, either of experimentally determined structures (solid symbols) or scaled assumed structures (open symbols). Dashed linear trends are shown for scaled experimentally determined structures of q-GeO_2 [43], FeS_2-like [19], and α-PbO_2-like GeO_2 [19,54], and for the scaled potential extreme-pressure CN = 9 structure of $PbCl_2$-like GeO_2 (violet) [13]. Isostructural compression decreases ΔE, as indicated by the dashed lines of negative slope for each structure. Between ΔE of the fourfold, sixfold, and ninefold coordinated structures lies a decrease of 0.25 eV on average. Thus, the position of the $K\beta''$ EL with respect to $K\beta_5$ reflects the germanium CN. The sequence of the four crystalline octahedral polymorphs results in isostructurally continuous weak decrease and additional stepwise decrease across structural transitions. The solid light red line represents the linear average of this structural evolution toward increasing octahedral distortion.
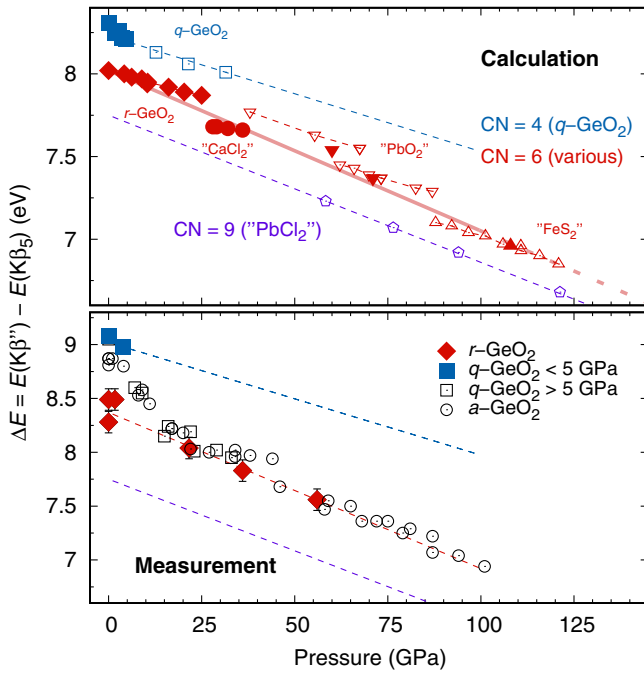
FIG. 4. Energy difference ΔE between the $K\beta''$ and $K\beta_5$ ELs as a function of pressure. Top: ΔE from Bethe-Salpeter equation spectral calculations of the sequence of crystalline high-pressure GeO_2 polymorphs with CN of six (solid red symbols), q-GeO_2 with CN of four (solid blue squares), scaled q-GeO_2 (open blue squares), and scaled $PbCl_2$-like GeO_2 with CN of nine (open pentagons). Open symbols represent scaled structures with computed spectra and pressure. Dashed lines indicate trends of isostructural compression. The solid linear trend indicates increasing octahedral distortion at constant CN = 6. Bottom: Measured ΔE of compressed q-GeO_2, a-GeO_2, and r-GeO_2 up to 35, 101, and 56 GPa, respectively. The dashed lines represent trends of CN = 4, 6, and 9.

Figure 4 (bottom) shows the measured evolution of ΔE with pressure of q-GeO_2 up to 35 GPa, r-GeO_2 up to 56 GPa, and a-GeO_2 up to 101 GPa. The experimental values of ΔE have an estimated uncertainty of 0.1 eV, which is indicated for r-GeO_2 at all pressures but omitted otherwise for clarity. ΔE of both a-GeO_2 and q-GeO_2 decreases steeply from about 9.0 to about 8.1 at 20 GPa, changes slope and continues to decrease linearly, following the trend observed in the spectra of compressed r-GeO_2 (red dashed line), which transforms to the $CaCl_2$ structure at 25 GPa [43]. The blue and violet dashed lines indicate the expected trends of q-GeO_2 and $PbCl_2$-like GeO_2, scaled from the slope observed in the computed spectra (in Fig. 4, top).

The qualitative agreement between trends observed in computed and in measured spectra of GeO_2 reference structures is excellent and underlines the sensitivity of ΔE with respect to coordination. The quantitative agreement of ΔE and its high-pressure trend of r-GeO_2 is not sufficient to base the quantitative evaluation on computed spectra. We therefore calculated the average germanium

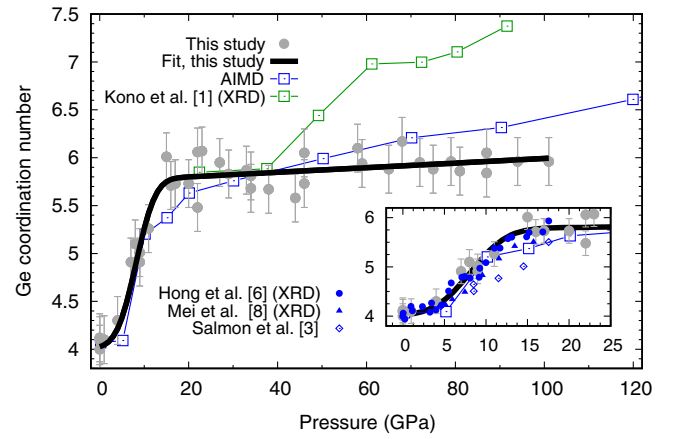FIG. 5. The average germanium CN in compressed q-GeO_2 and a-GeO_2 with literature data shown for comparison [1,3,6,8]. AIMD data are based on evaluation of the molecular dynamics results from Du and Tse [21]. The inset shows the pressure range up to 25 GPa, with additional literature data from XRD and neutron diffraction (ND) measurements.

CN of compressed a-GeO_2 and q-GeO_2 from measured ΔE, using as references for linear interpolation the measured high-pressure trend of r-GeO_2 from 0 to 56 GPa and the trend of q-GeO_2 (dashed lines in Fig. 4, bottom). The resulting CN and a general fit are shown in Fig. 5.

The rise of the average germanium CN from four at ambient pressure to six at about 20 GPa is in good agreement with other studies (see inset of Fig. 5) [1,3,6,8]. Above 20 GPa, the data indicate a persistent CN of six up to 100 GPa. This observation contrasts with results obtained from XRD by Kono *et al.*, who reported a steep rise between 40 and 60 GPa from CN = 6 to 7, followed by further increase to 7.4 at 91 GPa (green squares). In contrast, results from *ab initio* molecular dynamics (blue squares) rather strengthen the predominance of sixfold coordinated germanium up to 100 GPa. In Fig. 5, the data from Du and Tse were recalculated using the integration of the Ge-O $g(r)$ with a cutoff of 2.3 Å. In the original paper, a cutoff of 2.5 Å was used, which leads to inclusion of a small amount of second shell oxygen neighbors in the calculation of the CN [21].

The observed trend of ΔE, compared to those predicted for GeO_2 with CN of 4, 6, and 9, leaves little space for doubt about the persistence of sixfold coordination up to 100 GPa. The interpretation of the measured spectra in terms of Ge-O distance allows for an even deeper insight into the compaction mechanisms in amorphous GeO_2.

B. Ge-O distances

Imposed by the requirements described by bond-valence theory [40,41], the mean Ge-O distance of the structures of coordination numbers CN = 4, 6, and 9 have mean Ge-O distances significantly different from each other: 1.74 Å in fourfold coordinated q-GeO_2 at ambient pressure, between
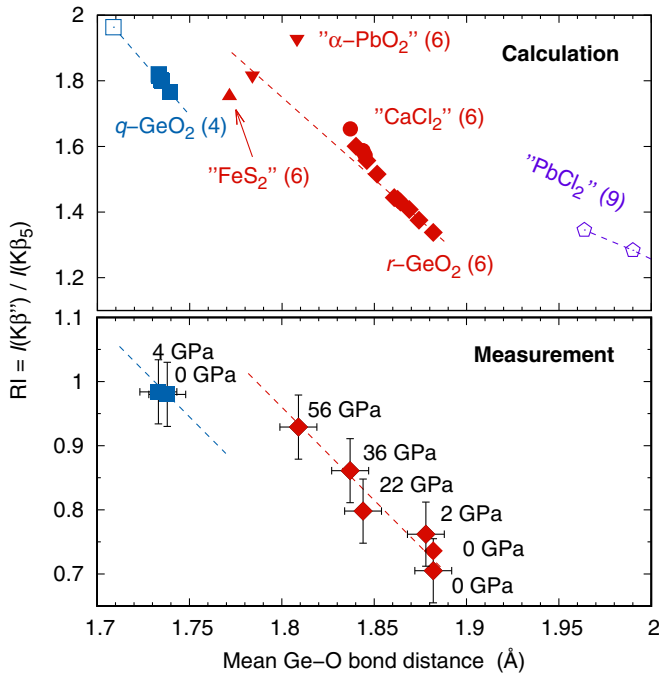
FIG. 6. Top: Computed RI from experimentally determined high-pressure structures (filled symbols) and scaled structures (open symbols). Numbers in parentheses indicate the CN. Bottom: Measured intensity parameter RI of compressed q-GeO$_2$ and r-GeO$_2$. Dashed lines represent linear trends.
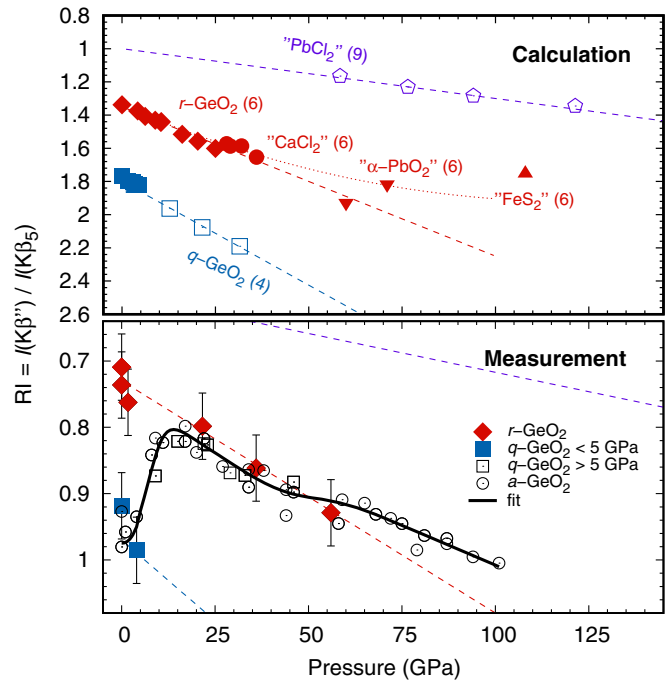

FIG. 7. Top: Computed RI of experimentally determined (solid symbols) and scaled (open symbols) high-pressure GeO$_2$ structures. Dashed lines indicate trends of CN = 4, 6, and 9. Bottom: Measured RI from a-GeO$_2$, q-GeO$_2$, and r-GeO$_2$, with linear trend of compressed r-GeO$_2$ (dashed line) and general fit to compressed q-GeO$_2$ and a-GeO$_2$ (solid curve). Error bars, indicated for r-GeO$_2$ and q-GeO$_2$, apply to all points.

1.88 and 1.85 Å in sixfold coordinated r-GeO$_2$ between ambient pressure and 25 GPa, 1.77 Å in FeS$_2$-like GeO$_2$ at 108 GPa, and 1.96 Å in ninefold coordinated PbCl$_2$-like GeO$_2$ at 120 GPa. This leads to three linear trends in RI as function of mean Ge-O distance, offset from each other by about 10% in computed spectra (Fig. 6, top).

Figure 6 (bottom) shows the measured RI of compressed q-GeO$_2$ and r-GeO$_2$. The experimental values of compressed r-GeO$_2$ up to 56 GPa follow a linear trend. Error bars in the bond length result from the uncertainty of the pressure measurement, those on RI represent the uncertainty from the fits to the measured spectra. As there is no high-pressure q-GeO$_2$ beyond 5 GPa, we assume a fourfold trend (blue dashed line) parallel to the sixfold trend (red dashed line), further constrained by RI of computed spectra.

We replot computed and measured RI as a function of pressure in Fig. 7 (top and bottom, respectively; note inverse y axis). In the computed results, the trends of fourfold, sixfold, and ninefold coordination are clearly offset from each other (top). The same applies to measured RI of q-GeO$_2$ and compressed r-GeO$_2$ (bottom). The trend in the computed RI sequence of sixfold coordination is almost linear up to 60 GPa (dashed red line, top). Above 60 GPa, data on experimentally determined structures is scarce and scattered, which leads to scatter in RI (compare, e.g., two RI values of α-PbO$_2$-like GeO$_2$ from two different studies [19,54]). We plot a nonlinear trend for comparison.

Experimental RI values of r-GeO$_2$ up to 56 GPa plot on a linear trend. Upon initial compression to 20 GPa, the measured RI values of a-GeO$_2$ and q-GeO$_2$ decrease at first, then follow the sixfold trend, with a slight change in slope around 50 GPa. We fit these data (disregarding three outliers at 44, 58, and 79 GPa) by two error functions and two linear trends, one below 55 GPa and one above. The computed trends of q-GeO$_2$ and PbCl$_2$-like GeO$_2$ (blue and violet dashed line, respectively) have been scaled in onset and slope, such that the trends of measured and computed spectra of r-GeO$_2$ match.

We convert the fit of measured RI values of compressed amorphous GeO$_2$ to mean Ge-O distances as a function of pressure, between linear RI trends of fourfold and sixfold coordination (Fig. 7). The resulting curve of mean Ge-O distance in compressed amorphous GeO$_2$ is shown in Fig. 8 (black line), together with important information on the bond lengths of crystalline polymorphs. Also shown are Ge-O distances in amorphous GeO$_2$, obtained from other techniques as reported in the literature. The estimated uncertainty of the average Ge-O distance is 0.02 Å and results mainly from the uncertainty of the function describing the trend of the Ge-O distance in the known crystalline sixfold polymorphs (red curve in Fig. 8). If instead of the red curve a linear fit to crystalline mean Ge-O distances is used as basis (not shown), the resulting Ge-O distance
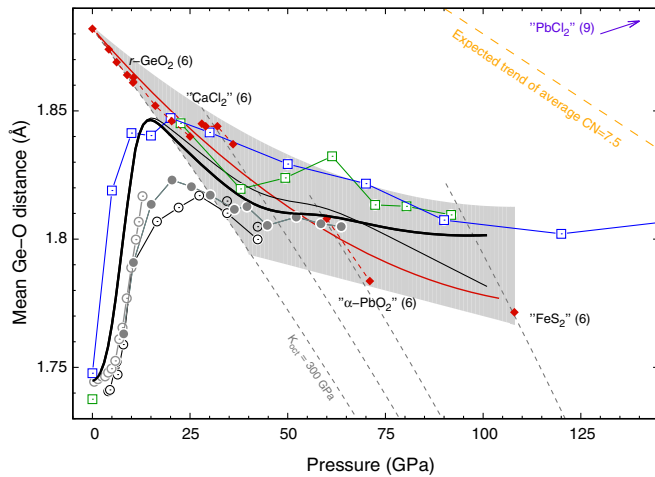
FIG. 8. Mean Ge-O distances as a function of pressure for compressed amorphous GeO_2 (black curve, this study) compared to mean Ge-O distances of octahedral crystalline high-pressure GeO_2 polymorphs (red solid symbols) [19,43,54,55] and to literature data on compressed amorphous GeO_2 from Kono *et al.* (XRD, green squares) [1], Du and Tse (AIMD, blue squares) [21], and three EXAFS studies (circles) [5,10,11]. Gray dashed lines indicate the isostructural compression trend described by a GeO_6 octahedral bulk modulus of 300 GPa [42]. The gray shaded area indicates qualitatively the area of octahedral coordination. The expected trend of average $CN = 7.5$, calculated as linear intermediate between $CN = 6$ and 9, is indicated (dashed orange line).

differs especially at high pressures, as shown by a second curve (thin black line). In the pressure region below 5 GPa, RI of compressed q-GeO_2 increases, whereas in amorphous GeO_2, RI decreases from the beginning, pointing to an earlier onset of coordination increase in amorphous GeO_2 compared to q-GeO_2, in line with a similar observation in EXAFS measurements of Ge-O distance [5].

The mean Ge-O distances of the sequence of sixfold coordinated GeO_2 are shown in red, together with a monotonic fit (red line), required for conversion of RI to Ge-O distance, as described above. Isostructural compression of any of these structures follows trends dictated by the GeO_6 octahedral bulk modulus of about 300 GPa [42] (four dashed gray lines in Fig. 8). They are tangential to the isostructural mean Ge-O distances (see, e.g., r-GeO_2 and α-PbO_2-like GeO_2). Starting from experimentally determined points of mean Ge-O distances, they extend to higher pressures, describing the expected *isostructural* evolution of Ge-O distances. However, the effective compression across structural transitions in the octahedral sequence from r-GeO_2 to FeS_2-like GeO_2 (red line) involves increasing octahedral distortion and thus allows for a much higher effective octahedral bulk modulus. The evolution of Ge-O distances in $PbCl_2$-like GeO_2 falls outside the range of the figure, being 1.96 Å at 120 GPa and 2.03 Å at 60 GPa. Instead, the trend of average

coordination number 7.5, calculated as the linear intermediate between $CN = 6$ and 9, is shown.

Our Ge-O distance values increase from 1.75 Å at ambient pressure to 1.85 Å at completion of the fourfold to sixfold coordination transition at 20 GPa, and decrease alongside the trend of effective crystalline octahedral compression up to about 50 GPa, from where on the bond length of amorphous GeO_2 decreases slower and exceeds those of the effective octahedral trend in the crystalline high-pressure sequence. The bond length between 90 and 100 GPa is 1.8 Å, 0.02 Å above the one of the crystalline polymorphs at the same pressure, but in good agreement with FeS_2-like GeO_2 determined at 108 GPa [19] when the isostructural compressibility of the GeO_6 octahedron is taken into account (rightmost gray dashed line). We take this agreement as an indicator for the FeS_2-like octahedral distortion in sixfold coordinated amorphous GeO_2.

Earlier EXAFS studies did not exceed 70 GPa, but reported mean Ge-O distances in good agreement to ours, albeit somewhat lower [5,10,11]. Systematic differences in the absolute bond length between XRD and EXAFS are commonly reported (see, e.g., Ref. [56]), but changes or trends are usually consistent. The only EXAFS study with data above 50 GPa coincides with the mean Ge-O distance of crystalline polymorphs (red line) line between 55 and their highest pressure of 64 GPa (gray circles) [5]. The bond length reported by Kono *et al.* at 90 GPa is in line with our measurements, but the interpretation concerning the average CN is different; we observe a persistent sixfold coordination, while a mean CN of 7.4 was reported with XRD. The recent *ab initio* molecular dynamics study of Du and Tse [21], yielding mean germanium CN below 6.5 at 100 GPa, was evaluated for the present study in terms of Ge-O distance (blue open squares). They are about 0.02 Å larger than ours, but almost coincide with those of Kono *et al.* between 40 and 90 GPa. Figure 8 indicates that a CN of 7.4 at 90 GPa should correspond to a mean bond length of about 1.89 Å, far from any experimental observation.

The contradiction between similar bond lengths in our XES study, in the XRD study by Kono *et al.*, and in the AIMD study by Du and Tse (Fig. 8), but differing coordination number at 90 GPa between 6.0 in our data, 6.4 in the data of Du and Tse, and 7.4 in the data of Kono *et al.*, can be resolved by a closer look at the evolution of the measured mean Ge-O distance as a function of pressure. The mean Ge-O distances of the crystalline high-pressure GeO_2 polymorphs r-GeO_2, $CaCl_2$-like, α-PbO_2-like, and FeS_2-like GeO_2 fall on a curved trend (solid red symbols and red line in Fig. 8). The curvature reflects a stepwise increase in octahedral distortion between crystalline polymorphs (Fig. 1). Contrary to this curvature, the mean Ge-O distance of each individual polymorph closely follows a trend described by an octahedral bulk modulus of about 300 GPa (gray dashed lines) [42]. These compression trends, together with the crystalline mean Ge-O distances,

define the area of octahedral coordination (shaded gray area in Fig. 8). All measured Ge-O distance curves of crystalline and amorphous GeO_2 lie within this area (with a few outliers), regardless of the measurement technique. Thus, the bond length evolution provides evidence for persistent octahedral germanium coordination with increasing distortion.

A mean Ge-O distance consistent with an average CN of 7.0 or higher must plot above the gray shaded area, as indicated by the Ge-O distances of ninefold coordinated $PbCl_2$-like GeO_2, being 2.03 Å at 60 GPa and 2.00 Å at 90 GPa (above the limits of the graph in Fig. 8). Assuming linear bond length increase between sixfold and ninefold coordination, the trend of bond length in average 7.5-fold coordination is indicated by the dashed orange line. It plots significantly above any reported Ge-O distance, indicating that the average germanium coordination remains close to sixfold at least up to 100 GPa. Furthermore, the AIMD data by Du and Tse confirm our view: The predominant sixfold coordination up to 100 GPa (Fig. 5) leads to a mean Ge-O distance curve in excellent agreement with the Ge-O distances by Kono *et al.* (blue and green open squares in Fig. 8).

The average germanium CN as high as 7.0 at 60 GPa, reported by Kono *et al.* [1], is based on the integration of the first maximum of the total radial distribution function $g(r)$. The Ge CN might be overestimated due to contributions from the first O-O shell to the first peak of the total radial distribution function. Furthermore, the $g(r)$ analysis has to rely on extrapolations of the density of amorphous GeO_2, which are uncertain at high pressure [1]. The XES signal is independent of the abovementioned factors.

The persistent octahedral coordination in compressed amorphous GeO_2 up to 100 GPa, accompanied by increasing octahedral distortion, indicates that the local structure in compressed amorphous GeO_2 follows closely the one found in the sequence of stable crystalline high-pressure phases of GeO_2. This is consistent with a recent x-ray absorption spectroscopy study on shock compressed amorphous SiO_2 to several hundreds GPa [57], also indicating that the local structure in compressed amorphous SiO_2 follows closely the one found in the sequence of stable crystalline high-pressure phases. GeO_2 and SiO_2 undergo similar structural transitions, although at different pressures [20]. Finally, x-ray Raman scattering spectroscopy data and Brillouin scattering of compressed amorphous SiO_2 both indicate a persistent sixfold silicon coordination up to 120 GPa [15,17], which is at odds with a recent XRD study reporting average silicon CN above six [18].

VII. CONCLUSION

VTC XES spectra of amorphous GeO_2, quartzlike GeO_2, and rutilelike GeO_2 have been measured up to 101, 35, and 56 GPa, respectively. Evaluation of the emission energy and the intensity of the $K\beta''$ allowed us to track the

persistent sixfold coordination of germanium up to 100 GPa. The Ge-O distance, which is in excellent agreement with earlier published values from XRD and EXAFS measurements, indicates persistent octahedral coordination with increasing distortion, like that observed for the sequence of crystalline high-pressure GeO_2 polymorphs. We therefore conclude that on the atomic scale amorphous GeO_2 behaves similarly to the experimentally determined crystalline polymorphs. A density crossover between compressed amorphous GeO_2 and its high-pressure crystalline phases is therefore possible only on the basis of a higher average degree of octahedral distortion, but not on the basis of a coordination increase beyond six.

The $K\beta''$ EL evaluation scheme described here is a valuable approach to access both bond lengths and coordination in amorphous material at high pressure. The procedure requires measurements or computational spectra of reference materials. Factors that limit the $K\beta''$ EL as a sufficiently intense and separate peak are the overall signal-to-noise ratio and the core-hole lifetime broadening of the cation, if its atomic number is too high. However, systems that exhibit the $K\beta''$ EL as part of their VTC XES spectra are the compounds of $3d$ transition metals (or adjacent elements) with ligands from the second or third row of the periodic table. Thus, systems for which the described procedure may be valuable are investigated in a range of scientific fields, from metallic glasses and phase change materials doped with oxygen and nitrogen, nitrides, and oxynitrides for photocatalysis to thin functional amorphous oxide or sulfide films.

[1] Y. Kono, C. Kenney-Benson, D. Ikuta, Y. Shibazaki, Y. Wang, and G. Shen, *Ultrahigh-Pressure Polyamorphism in* GeO_2 *Glass with Coordination Number* > 6, Proc. Natl. Acad. Sci. U.S.A. **113,** 3436 (2016).

[2] A. Cunsolo, Y. Li, C. N. Kodituwakka, S. Wang, D. Antonangeli, F. Bencivenga, A. Batistoni, R. Verbeni, S. Tsutsui, A. Q. R. Baron, H.-K. Mao, D. Bolmatov, and Y. Q. Cai, *Signature of a Polyamorphic Transition in the THz Spectrum of Vitreous* GeO_2, Sci. Rep. **5,** 14996 (2015).

[3] P. S. Salmon, J. W. E. Drewitt, D. A. J. Whittaker, A. Zeidler, K. Wezka, C. L. Bull, M. G. Tucker, M. C. Wilding, M. Guthrie, and D. Marrocchelli, *Density-Driven Structural Transformations in Network Forming Glasses: A High-Pressure Neutron Diffraction Study of* GeO_2 *Glass up to 17.5 GPa*, J. Phys. Condens. Matter **24,** 415102 (2012).

[4] J. Dong, X. Zhang, Q. Zhang, Y. Wu, X. Wu, Z. Wu, and D. Chen, *Pressure-Induced Drastic Collapse of a High Oxygen Coordination Shell in Quartz-like* α-GeO_2, New J. Phys. **16,** 023022 (2014).

[5] X. Hong, M. Newville, T. S. Duffy, S. R. Sutton, and M. L. Rivers, *X-Ray Absorption Spectroscopy of* GeO_2 *Glass to 64 GPa*, J. Phys. Condens. Matter **26,** 035104 (2014).

[6] X. Hong, L. Ehm, and T. S. Duffy, *Polyhedral Units and Network Connectivity in* GeO_2 *Glass at High Pressure: An X-Ray Total Scattering Investigation*, Appl. Phys. Lett. **105,** 081904 (2014).

[7] K. Wezka, P. S. Salmon, A. Zeidler, D. A. J. Whittaker, J. W. E. Drewitt, S. Klotz, H. E. Fischer, and D. Marrocchelli, *Mechanisms of Network Collapse in* GeO_2 *Glass: High-Pressure Neutron Diffraction with Isotope Substitution as Arbitrator of Competing Models*, J. Phys. Condens. Matter **24,** 502101 (2012).

[8] Q. Mei, S. Sinogeikin, G. Shen, S. Amin, C. J. Benmore, and K. Ding, *High-Pressure X-Ray Diffraction Measurements on Vitreous* GeO_2 *under Hydrostatic Conditions*, Phys. Rev. B **81,** 174113 (2010).

[9] G. Lelong, L. Cormier, G. Ferlat, V. Giordano, G. S. Henderson, A. Shukla, and G. Calas, *Evidence of Five-fold-Coordinated Ge Atoms in Amorphous* GeO_2 *under Pressure Using Inelastic X-Ray Scattering*, Phys. Rev. B **85,** 134202 (2012).

[10] M. Baldini, G. Aquilanti, H.-k. Mao, W. Yang, G. Shen, S. Pascarelli, and W. L. Mao, *High-Pressure EXAFS Study of Vitreous* GeO_2 *up to 44 GPa*, Phys. Rev. B **81,** 024201 (2010).

[11] M. Vaccari, G. Aquilanti, S. Pascarelli, and O. Mathon, *A New EXAFS Investigation of Local Structural Changes in Amorphous and Crystalline* GeO_2 *at High Pressure*, J. Phys. Condens. Matter **21,** 145403 (2009).

[12] M. Micoulaut, L. Cormier, and G. S. Henderson, *The Structure of Amorphous, Crystalline and Liquid* GeO_2, J. Phys. Condens. Matter **18,** R753 (2006).

[13] H. Dekura, T. Tsuchiya, and J. Tsuchiya, *First-Principles Prediction of Post-Pyrite Phase Transitions in Germanium Dioxide*, Phys. Rev. B **83,** 134114 (2011).

[14] S. Petitgirard, W. J. Malfait, R. Sinmyo, I. Kupenko, L. Hennet, D. Harries, T. Dane, M. Burghammer, and D. C. Rubie, *Fate of* $MgSiO_3$ *Melts at Core-Mantle Boundary Conditions*, Proc. Natl. Acad. Sci. U.S.A. **112,** 14186 (2015).

[15] S. Petitgirard, C. J. Sahle, K. Weis, K. Gilmore, G. Spiekermann, J. S. Tse, M. Wilke, C. Cavallari, V. Cerantola, and C. Sternemann, *Magma Properties at Deep Earth's Conditions from Electronic Structure of Silica*, Geochem. Persp. Lett. **9,** 32 (2019).

[16] J. P. Itie, A. Polian, G. Calas, J. Petiau, A. Fontaine, and H. Tolentino, *Pressure-Induced Coordination Changes in Crystalline and Vitreous* GeO_2, Phys. Rev. Lett. **63,** 398 (1989).

[17] M. Murakami and J. D. Bass, *Spectroscopic Evidence for Ultrahigh-Pressure Polymorphism in* SiO_2 *Glass*, Phys. Rev. Lett. **104,** 025504 (2010).

[18] C. Prescher, V. B. Prakapenka, J. Stefanski, S. Jahn, L. B. Skinner, and Y. Wang, *Beyond Sixfold Coordinated Si in* SiO_2 *Glass at Ultrahigh Pressures*, Proc. Natl. Acad. Sci. U.S.A. **114,** 10041 (2017).

[19] K. Shiraki, T. Tsuchiya, and S. Ono, *Structural Refinements of High-Pressure Phases in Germanium Dioxide*, Acta Crystallogr. Sect. B **59,** 701 (2003).

[20] V. B. Prakapenka, G. Shen, L. S. Dubrovinsky, M. L. Rivers, and S. R. Sutton, *High Pressure Induced Phase Transformation of* SiO_2 *and* GeO_2: *Difference and Similarity*, J. Phys. Chem. Solids **65,** 1537 (2004).

[21] X. Du and J. S. Tse, *Oxygen Packing Fraction and the Structure of Silicon and Germanium Oxide Glasses*, J. Phys. Chem. **121,** 10726 (2017).

[22] T. Sato and N. Funamori, *High-Pressure Structural Transformation of* SiO_2 *Glass up to 100 GPa*, Phys. Rev. B **82,** 184102 (2010).

[23] M. Wu, Y. Liang, J.-Z. Jiang, and J. S. Tse, *Structure and Properties of Dense Silica Glass*, Sci. Rep. **2,** 398 (2012).

[24] S. Petitgirard, W. J. Malfait, B. Journaux, I. E. Collings, E. S. Jennings, I. Blanchard, I. Kantor, A. Kurnosov, M. Cotte, T. Dane, M. Burghammer, and D. C. Rubie, SiO_2 *Glass Density to Lower-Mantle Pressures*, Phys. Rev. Lett. **119,** 215701 (2017).

[25] U. Bergmann, C. R. Horne, T. J. Collins, J. M. Workman, and S. P. Cramer, *Chemical Dependence of Interatomic X-Ray Transition Energies and Intensities–A Study of Mn* $K\beta''$ *and* $K\beta_{2,5}$ *Spectra*, Chem. Phys. Lett. **302,** 119 (1999).

[26] P. Glatzel and U. Bergmann, *High Resolution 1s Core Hole X-Ray Spectroscopy in 3d Transition Metal Complexes—Electronic and Structural Information*, Coord. Chem. Rev. **249,** 65 (2005).

[27] K. M. Lancaster, Y. Hu, U. Bergmann, M. W. Ribbe, and S. DeBeer, *X-Ray Spectroscopic Observation of an Interstitial Carbide in* NifEN-*Bound FeMoco Precursor*, J. Am. Chem. Soc. **135,** 610 (2013).

[28] E. Gallo and P. Glatzel, *Valence to Core X-Ray Emission Spectroscopy*, Adv. Mater. **26,** 7730 (2014).

[29] M. Bauer, *HERFD-XAS and Valence-to-Core XES: New Tools to Push the Limits in Research with Hard X-Rays?*, Phys. Chem. Chem. Phys. **16,** 13827 (2014).

[30] S. E. Canton *et al.*, *Visualizing the Non-Equilibrium Dynamics of Photoinduced Intramolecular Electron Transfer with Femtosecond X-Ray Pulses*, Nat. Commun. **6,** 6359 (2015).

[31] J. K. Kowalska, A. W. Hahn, A. Albers, C. E. Schiewer, R. Bjornsson, F. A. Lima, F. Meyer, and S. DeBeer, *X-Ray Absorption and Emission Spectroscopic Studies of* $[L_2Fe_2S_2]^n$ *Model Complexes: Implications for the*

Experimental Evaluation of Redox States in Iron-Sulfur Complexes, Inorg. Chem. **55**, 4485 (2016).

[32] S. DeBeer and U. Bergmann, *X-Ray Emission Spectroscopic Techniques in Bioinorganic Applications*, Encyclopedia Inorg. Bioinorg. Chem., DOI: 10.1002/9781119951438.eibc2158 (2016).

[33] R. Zhang, H. Li, and J.-S. McEwen, *Chemical Sensitivity of Valence-to-Core X-Ray Emission Spectroscopy due to the Ligand and the Oxidation State: A Computational Study on Cu-SSZ-13 with Multiple* H_2O *and* NH_3 *Adsorption*, J. Phys. Chem. **121**, 25759 (2017).

[34] A. M. March *et al.*, *Probing Transient Valence Orbital Changes with Picosecond Valence-to-Core X-Ray Emission Spectroscopy*, J. Phys. Chem. **121**, 2620 (2017).

[35] J. Badro, V. V. Struzhkin, J. Shu, R. J. Hemley, H.-K. Mao, C. C. Kao, J.-P. Rueff, and G. Shen, *Magnetism in* FeO *at Megabar Pressures from X-Ray Emission Spectroscopy*, Phys. Rev. Lett. **83**, 4101 (1999).

[36] J. R. Vegelius, K. O. Kvashnina, M. Klintenberg, I. L. Soroka, and S. M. Butorin, Cu $K\beta_{2,5}$ *X-Ray Emission Spectroscopy as a Tool for Characterization of Monovalent Copper Compounds*, J. Analytic Atom. Spectrom. **27**, 1882 (2012).

[37] C. Weis, G. Spiekermann, C. Sternemann, M. Harder, G. Vankó, V. Cerantola, C. J. Sahle, Y. Forov, R. Sakrowski, I. Kupenko, S. Petitgirard, H. Yava, C. Bressler, W. Gawelda, M. Tolan, and M. Wilke, *Combining X-Ray* $K\beta_{1,3}$, *Valence-to-Core, and X-Ray Raman Spectroscopy for Studying Earth Materials at High Pressure and Temperature: The Case of Siderite*, J. Analytical Atom. Spectrosc., DOI: 10.1039/C8JA00247A (2018).

[38] V. V. Struzhkin, H.-K. Mao, J.-F. Lin, R. J. Hemley, J. S. Tse, Y. Ma, M. Y. Hu, P. Chow, and C.-C. Kao, *Valence Band X-Ray Emission Spectra of Compressed Germanium*, Phys. Rev. Lett. **96**, 137402 (2006).

[39] R. Li, J. Liu, J. S. Tse, and G. Shen, *Pressure-Induced Changes in the Electron Density Distribution in* α-Ge *Near the* α-β *Transition*, Appl. Phys. Lett. **107**, 072109 (2015).

[40] I. D. Brown and D. Altermatt, *Bond-Valence Parameters Obtained from a Systematic Analysis of the Inorganic Crystal-Structure Database*, Acta Crystallogr. Sect. B **41**, 244 (1985).

[41] I. D. Brown, *Bond-Valence Parameters Obtained from a Systematic Analysis of the Inorganic Crystal-Structure Database*, Chem. Rev. **109**, 6858 (2009).

[42] R. M. Hazen and L. W. Finger, *Bulk Modulus-Volume Relationship for Cation-Anion Polyhedra*, J. Geophys. Res. **84**, 6723 (1979).

[43] J. Haines, J. M. Leger, C. Chateau, and A. S. Pereira, *Structural Evolution of Rutile-Type and* $CaCl_2$*-Type Germanium Dioxide at High Pressure*, Phys. Chem. Miner. **27**, 575 (2000).

[44] K. Momma and F. Izumi, *VESTA 3 for Three-Dimensional Visualization of Crystal, Volumetric and Morphology Data*, J. Appl. Crystallogr. **44**, 1272 (2011).

[45] J. A. Tossell, *The Electronic Structures of Silicon, Aluminum, and Magnesium in Tetrahedral Coordination with Oxygen from* SCF-Xα MO *Calculations*, J. Am. Chem. Soc. **97**, 4840 (1975).

[46] L. Mandić, S. Fazinić, and M. Jaksić, *Chemical Effects on the* Kβ″ *and* $K\beta_{2,5}$ *X-Ray Lines of Titanium and Its Compounds*, Phys. Rev. A **80**, 042519 (2009).

[47] A. Masuno, Y. Watanabe, H. Inoue, Y. Arai, J. Yu, and M. Kaneko, *Glass-Forming Region and High Refractive Index of* TiO_2*-Based Glasses Prepared by Containerless Processing*, Phys. Status Solidi C **9**, 2424 (2012).

[48] E. Kulik, N. Nishiyama, A. Masuno, Y. Zubavichus, V. Murzin, E. Khramov, A. Yamada, H. Ohfuji, H.-C. Wille, T. Irifune, and T. Katsura, *A Complete Solid Solution with Rutile-Type Structure in* SiO_2-GeO_2 *System at 12 GPa and* 1600 °C, J. Am. Ceram. Soc. **98**, 4111 (2015).

[49] H. K. Mao, P. M. Bell, J. W. Shaner, and D. J. Steinberg, *Specific Volume Measurements of* Cu, Mo, Pd, *and* Ag *and Calibration of the Ruby R1 Fluorescence Pressure Gauge from 0.06 to 1 Mbar*, J. Appl. Phys. **49**, 3276 (1978).

[50] R. Alonso-Mori, J. Kern, D. Sokaras, T. C. Weng, D. Nordlund, R. Tran, P. Montanez, J. Delor, V. K. Yachandra, J. Yano, and U. Bergmann, *A Multi-Crystal Wavelength Dispersive X-Ray Spectrometer*, Rev. Sci. Instrum. **83**, 073114 (2012).

[51] K. Gilmore, J. Vinson, E. L. Shirley, D. Prendergast, C. D. Pemmaraju, J. J. Kas, F. D. Vila, and J. J. Rehr, *Efficient Implementation of Core-Excitation Bethe-Salpeter Equation Calculations*, Comput. Phys. Commun. **197**, 109 (2015).

[52] P. Giannozzi *et al.*, *Advanced Capabilities for Materials Modelling with Quantum ESPRESSO*, J. Phys. Condens. Matter **29**, 465901 (2017).

[53] T. Yamanaka and K. Ogata, *Structure Refinement of* GeO_2 *Polymorphs at High Pressures and Temperatures by Energy-Dispersive Spectra of Powder Diffraction*, J. Appl. Crystallogr. **24**, 111 (1991).

[54] V. B. Prakapenka, L. S. Dubrovinsky, G. Shen, M. L. Rivers, S. R. Sutton, V. Dmitriev, H.-P. Weber, and T. L. Bihan, α-PbO_2*-Type High-Pressure Polymorph of* GeO_2, Phys. Rev. B **67**, 132101 (2003).

[55] S. Ono, T. Tsuchiya, K. Hirose, and Y. Ohishi, *High-Pressure form of Pyrite-Type Germanium Dioxide*, Phys. Rev. B **68**, 014103 (2003).

[56] M. Wilke, *Advances in High-Pressure Experiments on Structure and Properties of Melts: X-Ray Absorption Spectroscopy Measurements*, in *Magmas Under Pressure*, edited by Y. Kono and C. Sanloup (Elsevier, New York, 2018).

[57] A. Denoeud, S. Mazevet, F. Guyot, F. Dorchies, J. Gaudin, A. Ravasio, E. Brambrink, and A. Benuzzi-Mounaix, *High-Pressure Structural Changes in Liquid Silica*, Phys. Rev. E **94**, 031201 (2016).